Nanosheets

DOI: 10.1002/anie.201204208

An Effective Method for the Fabrication of Few-Layer-Thick Inorganic Nanosheets**

*Zhiyuan Zeng, Ting Sun, Jixin Zhu, Xiao Huang, Zongyou Yin, Gang Lu, Zhanxi Fan, Qingyu Yan, Huey Hoon Hng, and Hua Zhang**

Two-dimensional (2D) nanomaterials have been receiving great attention owing to their unique properties and potential applications in electronics and catalysis.[1,2] Besides graphene, inorganic 2D materials such as hexagonal boron nitride (h-BN) and transition-metal chalcogenides (TMCs) are reported to show also novel mechanical,[3] optical,[4] and thermoelectric properties.[5] For example, $NbSe_2$ and h-BN have been extensively studied and applied in, for example, light-emitting diodes,[6] magnetic flux,[7] and dielectric layers.[8] Since the interactions between the layers of the bulk material are determined by van der Waals forces, the mechanical cleavage method, for which scotch tapes are used, has been applied to fabricate single and few-layer-thick $NbSe_2$ nanosheets.[9] However, this method is restricted to the large-amount production of nanosheets. Alternatively, the other exfoliation-based methods or the direct growth of single or few-layer-thick 2D materials have been developed.[10–12]

BN nanosheets can be obtained from direct sonication of bulk h-BN crystals in different solvents, such as *N*,*N*-dimethylformamide (DMF),[3] a mixture of ethanol and water,[13] a mixture of 1,2-dichloroethane and poly(phenylenevinylene) polymer,[14] and a solution of the Lewis base octadecylamine (OD).[15] In the aforementioned articles,[3,13–15] the strong affinity of the organic molecules or solvents on the h-BN surface weakened the van der Waals interaction between the adjacent BN layers and thus facilitated the exfoliation and isolation of the individual nanosheets upon sonication. To prepare the $NbSe_2$ nanosheets, direct sonication of bulk $NbSe_2$ crystals in organic solvents[16] and sodium cholate/water solution[17] as well as an intercalation-assisted thermal cleavage method[18,19] have been reported. Recently, we developed a simple and effective method to prepare single-layer 2D nanosheets, such as MoS_2, WS_2, TiS_2, TaS_2, ZrS_2, and graphene, through a controllable process of lithium intercalation and subsequent sonication and exfoliation of the lithium-intercalated compounds in water or ethanol.[20] However, there is a big challenge to simply apply this lithium intercalation process to prepare other types of 2D materials, such as h-BN and metal selenides or tellurides (e.g. $NbSe_2$, WSe_2, Sb_2Se_3, and Bi_2Te_3). Unlike the previously reported transition-metal sulfide crystals, which showed a distinct discharge plateau during the electrochemical lithium intercalation process, the h-BN and metal selenides or tellurides give continuously descending discharge curves without a plateau. This makes it difficult to determine the cut-off voltage (i.e. the voltage at which the discharge stops) to obtain the optimized Li amount inserted in the bulk materials. The insufficient insertion of Li can lead to ineffective exfoliation, while too much insertion of Li will result in the chemical decomposition of the crystals.[20]

In this contribution, we have successfully optimized the electrochemical lithium intercalation conditions for the preparation of few-layer-thick BN, $NbSe_2$, WSe_2, Sb_2Se_3, and Bi_2Te_3 nanosheets through a systematic examination of the nanomaterials obtained at different cut-off voltages. More importantly, we have employed two approaches to improve the quality of the products, that is, we use a low discharge current to prevent high-current-induced structure degradation and the deoxygenation of the lithium-intercalated compound solutions to alleviate the surface oxidation of the nanosheets during sonication. As a proof of concept, the thermoelectric properties of the $NbSe_2$ nanosheet films were tested, which showed both electrical p-type semiconductivity and an enhanced Seebeck coefficient relative to the bulk material.

Scheme 1 shows the electrochemical lithium intercalation process used to prepare the 2D nanosheets. First, the layered bulk material is mixed with acetylene black and a poly(vinylidene fluoride) (PVDF) binder dispersed in *N*-methylpyrrolidone (NMP). The mass ratio of the layered bulk material, acetylene black, and PVDF in the mixed slurry is 80:10:10. The resulting slurry is then uniformly coated on a copper foil and dried in vacuum at 100 °C overnight (Scheme 1 a). Then, the bulk material-coated Cu foil used as the cathode, the lithium foil used as the anode, and the polypropylene (PP) film used as the separator are assembled into a lithium ion battery in an Ar-filled glove box, with 1 M $LiPF_6$ in a mixture of ethylene carbonate (EC) and dimethyl carbonate (DMC)

[*] Z. Y. Zeng, Dr. T. Sun, Dr. J. X. Zhu, Dr. X. Huang, Dr. Z. Y. Yin, Dr. G. Lu, Z. X. Fan, Prof. Q. Y. Yan, Prof. H. H. Hng, Prof. H. Zhang
School of Materials Science and Engineering
Nanyang Technological University
50 Nanyang Avenue, Singapore 639798 (Singapore)
E-mail: hzhang@ntu.edu.sg
hzhang166@yahoo.com
Homepage: http://www.ntu.edu.sg/home/hzhang/
Dr. J. X. Zhu, Prof. Q. Y. Yan
TUM CREATE Centre for Electromobility
Nanyang Technological University
Singapore 637459 (Singapore)

[**] The authors gratefully acknowledge the financial support from the MOE under AcRF Tier 2 (ARC 10/10, grant number MOE2010-T2-1-060), the Singapore National Research Foundation under CREATE program: Nanomaterials for Energy and Water Management, and the NTU under the start-up grant (number M4080865.070.706022) in Singapore.

Supporting information for this article is available on the WWW under http://dx.doi.org/10.1002/anie.201204208.

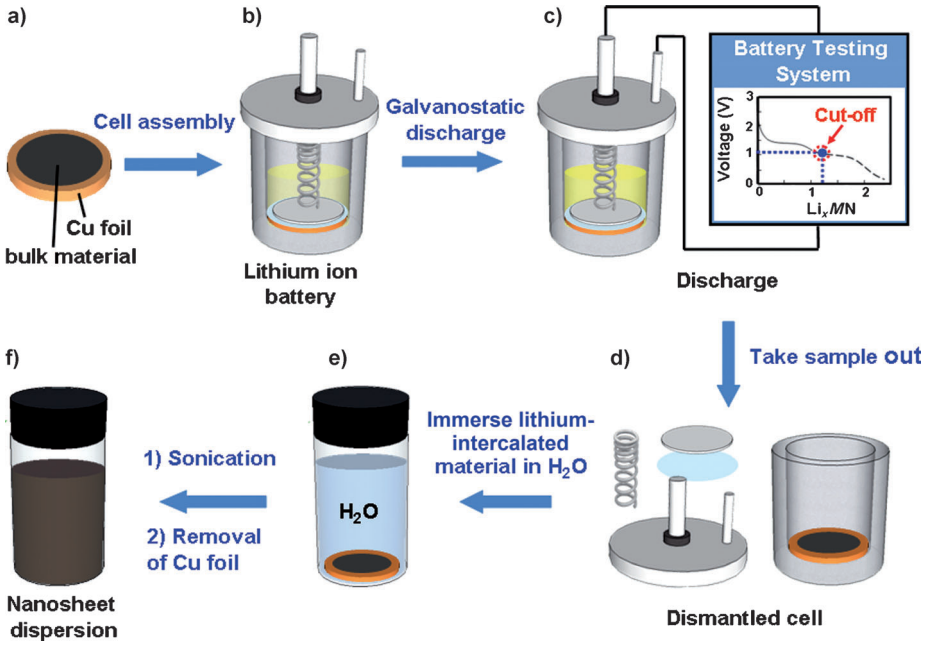

Scheme 1. The electrochemical lithium intercalation process to produce 2D nanosheets from the layered bulk material (*MN* = BN, metal selenides, or metal tellurides in Li_xMN).

(v:v = 1:1) as electrolyte (Scheme 1 b). The obtained battery cell is connected to a Neware battery test system at room temperature. The electrochemical lithium intercalation is performed through the galvanostatic discharge at a current of 0.025 mA (Scheme 1 c). By optimizing the cut-off voltage (or the discharge capacity), we can control the amount of the Li ions intercalated between the layers of the bulk material, so that the Li insertion process can stop at a proper Li amount to avoid the decomposition of the lithium-intercalated compound. After the lithium intercalation, the battery cell is dismantled (Scheme 1 d) and the lithium-intercalated material, coated on the Cu foil, is taken out, rinsed with acetone to remove the residual electrolyte (i.e. $LiPF_6$), and dried. Finally, the lithium-intercalated material on Cu foil is immersed in Milli-Q water deoxygenated with N_2 in a closed vial (Scheme 1 e) and subsequently sonicated for 10 minutes. During the sonication, the profuse evolution of gas can be observed and an opaque suspension of the exfoliated materials formed (Scheme 1 f). During the whole experimental process, the lithium ions fulfill several important functions. First, the Li^+ ions are inserted into the interlayer space of the layered bulk material, which expands the interlayer distance and weakens the van der Waals interactions between the layers. Second, the inserted Li^+ ions are subsequently reduced to Li^0 by accepting electrons during the discharge process. The metallic Li can react with water to form LiOH and produce H_2 gas (evidently, bubbles were observed during our experiments).[21,22] The generated H_2 gas pushes the layers further apart. Under vigorous agitation by sonication, well-dispersed 2D nanosheets are thus obtained.

Figure 1 a shows the transmission electron microscopy (TEM) image of a typical h-BN nanosheet. The selected area electron diffraction (SAED) pattern (inset in Figure 1 a) of the flat area of the nanosheet and the high-resolution TEM (HRTEM) image (Figure 1 b) indicate the hexagonal lattice structure. A lattice spacing of 2.2 Å can be assigned to the BN (100) planes.[23] The folded edges of typical double- (Figure 1 c) and triple-layer (Figure 1 d) BN nanosheets show the interlayer spacing of 3.3 Å, which is in agreement with the theoretic value of the bulk h-BN.[23] The TEM image and SAED pattern of the obtained $NbSe_2$ nanosheet are shown in Figure 1 e. The lattice spacing of 3.0 Å shown in the HRTEM image (Figure 1 f) is consistent with that of the $NbSe_2$ (100) plane. The photographs of the BN and $NbSe_2$ solutions are shown in Figure 1 g and 1 h, respectively, indicating the production of homogeneous dispersions of the 2D materials by using our method.

Scanning electron microscopy (SEM) and atomic force microscopy (AFM) were used to further characterize the morphology and thickness of these 2D nanomaterials. Figure 2 a–c shows SEM images of BN nanosheets deposited on Si/SiO_2 substrates with a lateral size up to 550, 670, and 730 nm, respectively. Their thicknesses of 2.3, 4.0 and 8.0 nm (Figure 2 d–f) are determined by AFM measurements, confirming that few-layer-thick BN nanosheets were successfully

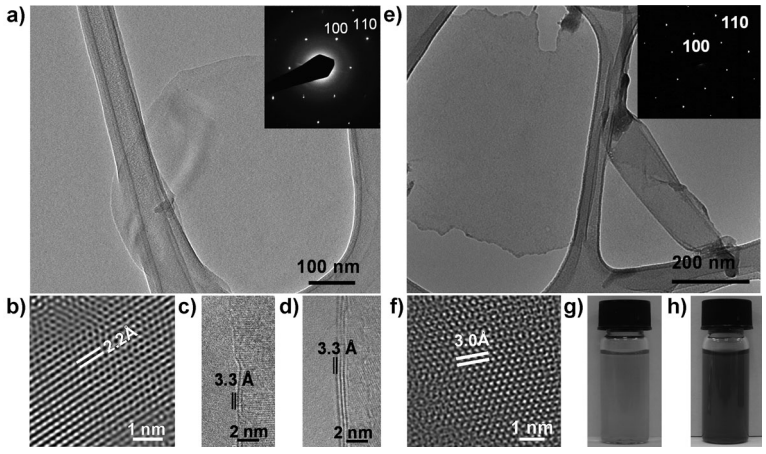

Figure 1. a) TEM image of a typical BN nanosheet. Inset: SAED pattern of the BN nanosheet. b) HRTEM image of few-layer-thick BN nanosheet. c–d) TEM images of the folded edges of c) double- and d) triple-layered BN nanosheets. e) TEM image of a typical $NbSe_2$ nanosheet. Inset: SAED pattern of the $NbSe_2$ nanosheet. f) HRTEM image of a few-layer-thick $NbSe_2$ nanosheet. Photographs of g) the BN solution and h) the $NbSe_2$ solution.

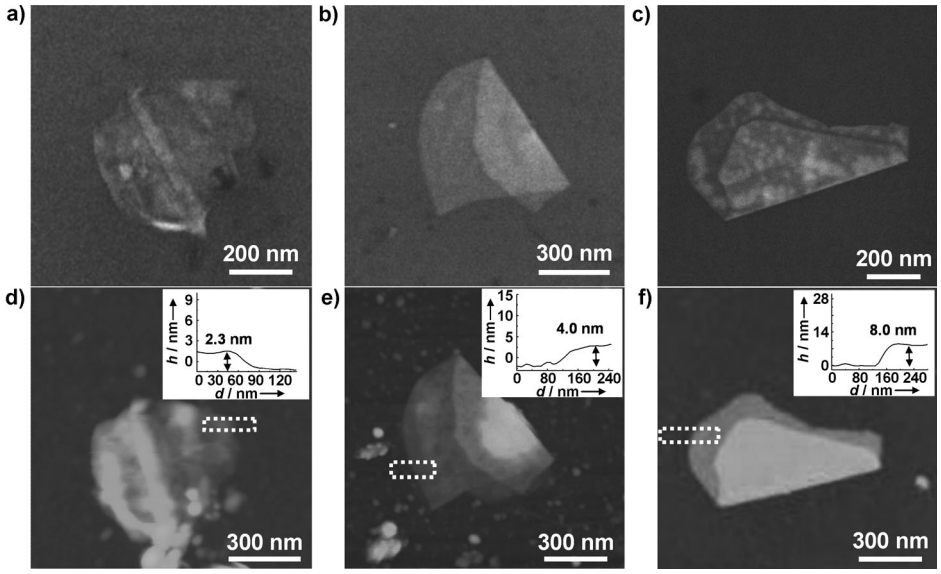

Figure 2. SEM images of typical BN nanosheets deposited on Si/SiO_2 substrates with a lateral size up to a) 550, b) 670, and c) 730 nm. AFM measurements of the corresponding BN nanosheets in (a–c) give the thickness of d) 2.3, e) 4.0, and f) 8.0 nm, confirming that few-layer-thick BN nanosheets were successfully produced.

fabricated by using our method. The chemical composition of the obtained BN nanosheets was studied by X-ray photoelectron spectroscopy (XPS, see Figure S1 in the Supporting Information). The B1s spectrum can be fitted by two energy bands at 189.1 and 190.4 eV, the N1s peak can be fitted with two subbands located at 396.3 and 397.5 eV, which may be assigned to B1s and N1s oxidation states in $Li_\delta BN$ (δ is the residual amount of Li ions on BN nanosheet)[24,25] and BN, respectively.[24,26,27]

The SEM images in Figure 3 a,b show that we have successfully prepared the micron-size $NbSe_2$ nanosheets with lateral sizes up to 6.4 μm. The AFM measurements further indicate that the obtained few-layer-thick $NbSe_2$ nanosheets have thickness of 2–3 nm (Figure 3 c,d). To the best of our knowledge, this is the first time that AFM images are used as direct evidence for the formation of few-layer-thick $NbSe_2$ nanosheets, which further proves the effectiveness of our method. The XPS spectra of Nb3d and Se3d core peaks are shown in Figure S2 in the Supporting Information. The doublet with components at 203.8 and 206.5 eV is attributed to $Nb^{(4-\varepsilon)+}$ in $Li_\varepsilon NbSe_2$ (ε is the residual amount of Li ions intercalated on $NbSe_2$ nanosheet).[25,28] The two bands at 204.4 and 207.2 eV are assigned to Nb^{4+} ions in $NbSe_2$. Those at 208.1 and 210.9 eV are attributed to Nb^{5+} ions in the oxidized species of Nb_2O_5.[28] For the evolution of the Se3d core peak, the doublet (54.6–55.5 eV) corresponds to Se^{2-} ions in $NbSe_2$, indicating that selenium is not oxidized.[28,29]

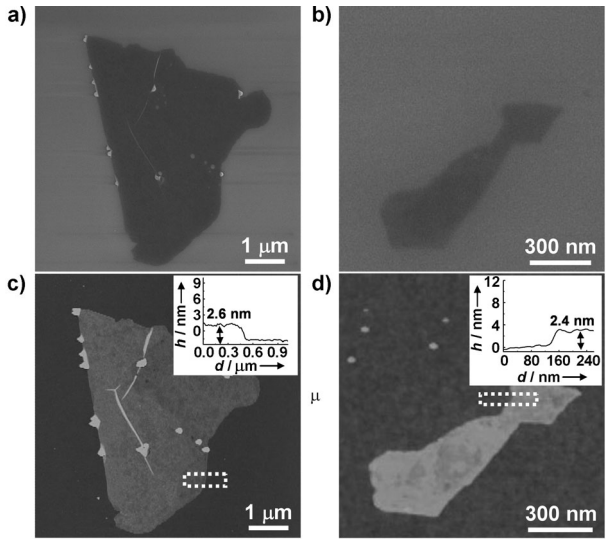

Figure 3. SEM images of typical $NbSe_2$ nanosheets deposited on Si/SiO_2 substrates with lateral size up to a) ~6.4 and b) 1.1 μm. The corresponding AFM measurements of $NbSe_2$ nanosheets give the thickness of c) 2.6 and d) 2.4 nm, confirming that few-layer-thick $NbSe_2$ nanosheets were successfully produced.

Compared to the traditional lithium intercalation method which uses the expensive *n*-butyllithium as the intercalating agent, our method requires an elevated reaction temperature and takes long time,[22] our electrochemical lithium intercalation method can be easily conducted at room temperature and is well-controlled.[20] However, unlike our previously reported transition-metal sulfide crystals (e.g. MoS_2, WS_2 and TiS_2) which showed distinct discharge plateaus during the electrochemical lithium intercalation process, the h-BN and metal selenide or telluride materials show a continuously descending discharge curve without a plateau. The lack of a plateau makes it difficult to determine the cut-off voltage (i.e. the voltage at which the discharge stops) to obtain the optimized amount of inserted Li ions. Therefore, in the present work, to apply the lithium intercalation method to BN and $NbSe_2$, as well as to other layered materials, we determined the optimized cut-off voltage by carrying out a series of control experiments at different discharge capacities and systematically examined the obtained products.

Taking h-BN as an example, its galvanostatic discharge curve (i.e. open circuit voltage vs. x, where x is the number of Li atoms in Li_xBN) shows that the cell voltage decreases from 1.8 to 0.4 V (at $0 < x < 0.058$) without an obvious discharge plateau (Figure S3 a in the Supporting Information). The optimized cut-off voltage is 0.4 V. If the discharge was stopped at a voltage higher than 0.4 V, only thick BN flakes were obtained. On the other hand, if the discharge was continued till 0.3 V, chemical decomposition of BN crystals was observed (Figure S4 in the Supporting Information). A discharge curve with a similar profile was also observed for $NbSe_2$ crystals (Figure S3 b in the Supporting Information).

Based on our systematic study, the optimized intercalated lithium amount (x) in $NbSe_2$ for preparation of high-quality exfoliated $NbSe_2$ nanosheets was 3.2, corresponding to a discharge voltage of 0.7 V, where the lithium intercalation process stopped. Importantly, to further improve the quality of the produced nanosheets, we set, based on our systematical investigation, the discharge current at 0.025 mA, which is lower than the 0.05 mA used in our previous procedure.[20] Using this current, the structure degradation induced by a large discharge current can be avoided. Furthermore, we also applied a deoxygenation procedure by degasing the water solution of the lithium-intercalated compounds with N_2, to alleviate the excessive surface oxidation under sonication.

Most importantly, our current method based on the aforementioned technical improvement cannot only be used for fabrication of BN and $NbSe_2$ nanosheets, but also applied to a wide range of layered materials, such as WSe_2, Sb_2Se_3, and Bi_2Te_3. For example, Figure S5 in the Supporting Information shows the SEM images of WSe_2 powder and a WSe_2 nanosheet after exfoliation. Similarly, the SEM images of Sb_2Se_3 and Bi_2Te_3 before and after exfoliation are shown in Figures S6 and S7 in the Supporting Information, respectively. As observed, the Sb_2Se_3 and Bi_2Te_3 bulk materials are crystals, while the exfoliated materials show a sheet morphology, and appear darker in contrast to the Si/SiO_2 substrate in the SEM images, indicating the better electrical conductivity of the semiconducting nanosheets relative to the Si/SiO_2 substrate.

As a proof of concept for potential applications of the produced 2D materials, the thermoelectric properties of the $NbSe_2$ nanosheets were measured. Figure 4a shows the temperature-dependent Seebeck coefficient (or the thermoelectric power) for the $NbSe_2$ nanosheets and the bulk crystals. The bulk $NbSe_2$ gives a negative Seebeck coefficient, indicating its n-type semiconducting behavior. However, the Seebeck coefficient of the $NbSe_2$ nanosheets is positive, suggesting a p-type semiconducting behavior.[5,30] This is consistence with the results reported previously. The nanosheets obtained from lithium intercalation and exfoliation are p-type semiconductors.[5,31] In addition, the $NbSe_2$ nanosheets gave much higher absolute Seebeck coefficients (Figure 4a) and an increased electrical conductivity (Figure 4b) relative to the bulk counterpart, resulting in improved overall thermoelectric transport properties, in terms of the power factor, that is, $S^2\sigma$, (S = Seebeck coefficient, σ = electrical conductivity, Figure 4c). These enhanced properties can be ascribed to a change in the carrier concentration and mobility of $NbSe_2$ after lithium intercalation and exfoliation,[30] most likely caused by the extra electrons introduced into the half-filled Nb d_{z^2} band.[5,31]

In summary, we have prepared few-layer-thick BN, $NbSe_2$, WSe_2, Sb_2Se_3, and Bi_2Te_3 nanosheets from their layered bulk precursors by using an electrochemical lithium intercalation process. The lithium intercalation conditions, such as cut-off voltage and discharge current, have been systematically studied and optimized. The high-quality BN and $NbSe_2$ nanosheets, which were evidenced by SEM, TEM, and AFM, have been successfully produced. In addition, the $NbSe_2$ nanosheets showed both an enhanced Seebeck coefficient and an electrical p-type semiconductivity, suggesting their potential application in thermoelectric devices.

Experimental Section

Chemicals: Boron nitride (BN, Sigma, Steinheim, Germany), niobium selenide ($NbSe_2$, Alfa Aeser, Massachusetts, USA), tungsten(IV) selenide (WSe_2, Alfa Aeser, Massachusetts, USA), antimony triselenide (Sb_2Se_3, Sigma, Steinheim, Germany), bismuth telluride (Bi_2Te_3, Sigma, Steinheim, Germany), poly(vinylidene fluoride) (PVDF, Sigma, Steinheim, Germany), *N*-methylpyrrolidone (Sigma, Steinheim, Germany), lithium ion battery electrolyte (Charslton Technologies Pte Ltd., International Business Park, Singapore), lithium foil (ACME Research Support Pte Ltd, Bukit Batok Street, Singapore), polypropylene (PP) film (Celgard 2300, North Carolina, USA), copper foil (ACME Research Support Pte Ltd, Bukit Batok Street, Singapore), acetone (Tech Grade, Aik Moh Paints & Chemicals Pte Ltd, Singapore), ethanol (> 99.9%, Merck, Darmstadt, Germany) were used as received without further purification. The deionized water was purified using the Milli-Q system (Millipore, Billerica, MA, USA).

Electrochemical intercalation: The lithium intercalation of the layered material was performed in a test cell with the Li foil as anode and 1M $LiPF_6$ dissolved in the mixture of ethyl carbonate (EC) and dimethyl carbonate (DMC) (1:1 in volume ratio) as electrolyte. The layered bulk material (i.e. BN, $NbSe_2$, WSe_2, Sb_2Se_3 and Bi_2Te_3) was prepared as cathode by adding acetylene black and poly(vinylidene fluoride) (PVDF) binder dispersed in *N*-methylpyrrolidone (NMP) solutions. The mass ratio of the layered bulk material, acetylene black, and PVDF in the mixed slurry was 80:10:10. The resulting slurry was then uniformly coated on a copper foil and vacuum-dried at 100 °C overnight. The test cells for different layered materials were assembled in an Ar-filled glove box. The electrochemical intercalation (galvanostatic discharge) of the layered materials in the test cells was conducted in a Neware battery test system at a current density of 0.025 mA. After the discharge process, the lithium-intercalated

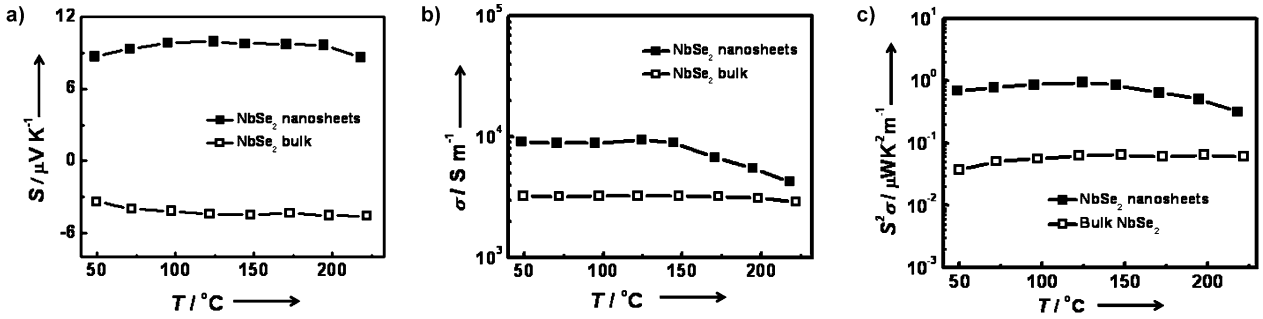

Figure 4. Temperature-dependent Seebeck coefficient (a), electrical conductivity (b), and powder factor (c) for $NbSe_2$ nanosheets and the bulk material.

sample was washed with acetone to remove the residual electrolyte ($LiPF_6$), followed by exfoliation and sonication in N_2-saturated Milli-Q water in a closed vial. During the experiment, the profuse evolution of gas was observed and an opaque suspension of the layered materials formed. After the suspension was centrifuged and washed six times with water, the solid product was collected for further characterizations.

Preparation and characterization of thermoelectric devices: After a glass slide was cleaned with ethanol, $NbSe_2$ nanosheets dispersed in ethanol was sprayed onto the glass substrate which was preheated at 80 °C. The thickness of the $NbSe_2$ nanosheet film was 0.5–0.6 μm, measured by the Alpha-Step IQ surface profiler. The resistivity and Seebeck coefficient were measured from 50 to 225 °C using a commercially available ZEM 3 Seebeck meter in helium atmosphere. The reference sample of bulk $NbSe_2$ was prepared by the following experiments. First, the commercial $NbSe_2$ powders (Sigma Aldrich) was kept at 10 MPa to form a 15 mm-diameter pellet. Then the pellet was cut to several small rectangular bars with dimensions of $14 \times 2 \times 2\ mm^3$, which were used as reference samples.

Characterizations: A drop of a solution containing the produced 2D nanosheets was placed on a holey carbon-coated copper grid and a Si/SiO_2 substrate and then naturally dried in air prior to characterization with transmission electron microscopy (TEM, JEM 2100F), scanning electron microscopy (SEM, JSM-7600F) coupled with energy dispersive X-ray spectroscopy (EDS), X-ray photoelectron spectroscopy (XPS, Axis Ultra), and atomic force microscopy (AFM, Dimension 3100 Veeco, CA, USA), respectively. The UV/Vis absorptions of the samples were examined using a UV spectrophotometer (UV-1800, Shimadzu, Japan).

Received: May 30, 2012
Published online: August 7, 2012

Keywords: boron nitride · electrochemistry · intercalations · metal chalcogenides · nanomaterials

[1] a) B. Radisavljevic, A. Radenovic, J. Brivio, V. Giacometti, A. Kis, *Nat. Nanotechnol.* **2011**, *6*, 147–150; b) X. Huang, X. Y. Qi, F. Boey, H. Zhang, *Chem. Soc. Rev.* **2012**, *41*, 666–686; c) X. Huang, Z. Y. Yin, S. X. Wu, X. Y. Qi, Q. Y. He, Q. C. Zhang, Q. Y. Yan, F. Boey, H. Zhang, *Small* **2011**, *7*, 1876—1902; d) X. Huang, Z. Y. Zeng, Z. X. Fan, J. Q. Liu, H. Zhang, *Adv. Mater.*, DOI: 10.1002/adma.201201587.

[2] R. R. Chianelli, M. H. Siadati, M. P. De La Rosa, G. Berhault, J. P. Wilcoxon, R. Bearden, B. L. Abrams, *Catal. Rev. Sci. Eng.* **2006**, *48*, 1–41.

[3] C. Y. Zhi, Y. Bando, C. C. Tang, H. Kuwahara, D. Golberg, *Adv. Mater.* **2009**, *21*, 2889–2893.

[4] a) Z. Y. Yin, H. Li, H. Li, L. Jiang, Y. M. Shi, Y. H. Sun, G. Lu, Q. Zhang, X. D. Chen, H. Zhang, *ACS Nano*, **2012**, *6*, 74–80; b) G. E. Myers, G. L. Montet, *J. Appl. Phys.* **1970**, *41*, 4642–4649.

[5] J. Heising, M. G. Kanatzidis, *J. Am. Chem. Soc.* **1999**, *121*, 11720–11732.

[6] K. J. Reynolds, G. L. Frey, R. H. Friend, *Appl. Phys. Lett.* **2003**, *82*, 1123–1125.

[7] U. Yaron, P. L. Gammel, D. A. Huse, R. N. Kleiman, C. S. Oglesby, E. Bucher, B. Batlogg, D. J. Bishop, K. Mortensen, K. Clausen, C. A. Bolle, F. De La Cruz, *Phys. Rev. Lett.* **1994**, *73*, 2748–2751.

[8] G. Giovannetti, P. A. Khomyakov, G. Brocks, P. J. Kelly, J. van den Brink, *Phys. Rev. B* **2007**, *76*, 073103.

[9] K. S. Novoselov, D. Jiang, F. Schedin, T. J. Booth, V. V. Khotkevich, S. V. Morozov, A. K. Geim, *Proc. Natl. Acad. Sci. USA* **2005**, *102*, 10451–10453.

[10] a) J. W. Seo, Y. W. Jun, S. W. Park, H. Nah, T. Moon, B. Park, J. G. Kim, Y. J. Kim, J. Cheon, *Angew. Chem.* **2007**, *119*, 8984–8987; *Angew. Chem. Int. Ed.* **2007**, *46*, 8828–8831; b) H. Li, Z. Y. Yin, Q. Y. He, H. Li, X. Huang, G. Lu, D. W. H. Fam, A. I. Y. Tok, Q. Zhang, H. Zhang, *Small* **2012**, *8*, 63–67.

[11] H. S. S. Matte, A. Gomathi, A. K. Manna, D. J. Late, R. Datta, S. K. Pati, C. N. R. Rao, *Angew. Chem.* **2010**, *122*, 4153–4156; *Angew. Chem. Int. Ed.* **2010**, *49*, 4059–4062.

[12] a) L. Song, L. J. Ci, H. Lu, P. B. Sorokin, C. H. Jin, J. Ni, A. G. Kvashnin, D. G. Kvashnin, J. Lou, B. I. Yakobson, P. M. Ajayan, *Nano Lett.* **2010**, *10*, 3209–3215; b) K. K. Liu, W. J. Zhang, Y. H. Lee, Y. C. Lin, M. T. Chang, C. Y. Su, C. S. Chang, H. Li, Y. M. Shi, H. Zhang, C. S. Lai, L. J. Li, *Nano Lett.* **2012**, *12*, 1538–1544.

[13] K.-G. Zhou, N.-N. Mao, H.-X. Wang, Y. Peng, H.-L. Zhang, *Angew. Chem.* **2011**, *123*, 11031–11034; *Angew. Chem. Int. Ed.* **2011**, *50*, 10839–10842.

[14] W. Q. Han, L. J. Wu, Y. M. Zhu, K. Watanabe, T. Taniguchi, *Appl. Phys. Lett.* **2008**, *93*, 223103.

[15] Y. Lin, T. V. Williams, J. W. Connell, *J. Phys. Chem. Lett.* **2010**, *1*, 277–283.

[16] J. N. Coleman, M. Lotya, A. O'Neill, S. D. Bergin, P. J. King, U. Khan, K. Young, A. Gaucher, S. De, R. J. Smith, I. V. Shvets, S. K. Arora, G. Stanton, H. Y. Kim, K. Lee, G. T. Kim, G. S. Duesberg, T. Hallam, J. J. Boland, J. J. Wang, J. F. Donegan, J. C. Grunlan, G. Moriarty, A. Shmeliov, R. J. Nicholls, J. M. Perkins, E. M. Grieveson, K. Theuwissen, D. W. McComb, P. D. Nellist, V. Nicolosi, *Science* **2011**, *331*, 568.

[17] R. J. Smith, P. J. King, M. Lotya, C. Wirtz, U. Khan, S. De, A. O'Neill, G. S. Duesberg, J. C. Grunlan, G. Moriarty, J. Chen, J. Wang, A. I. Minett, V. Nicolosi, J. N. Coleman, *Adv. Mater.* **2011**, *23*, 3944–3948.

[18] J.-M. Li, *Appl. Phys. A* **2010**, *99*, 229–235.

[19] H.-L. Tsai, J. L. Schindler, C. R. Kannewurf, M. G. Kanatzidis, *Chem. Mater.* **1997**, *9*, 875–878.

[20] Z. Y. Zeng, Z. Y. Yin, X. Huang, H. Li, Q. Y. He, G. Lu, F. Boey, H. Zhang, *Angew. Chem.* **2011**, *123*, 11289–11293; *Angew. Chem. Int. Ed.* **2011**, *50*, 11093–11097.

[21] B. K. Miremadi, S. R. Morrison, *J. Catal.* **1991**, *131*, 127–132.

[22] P. Joensen, R. F. Frindt, S. R. Morrison, *Mater. Res. Bull.* **1986**, *21*, 457–461.

[23] R. Pease, *Acta Crystallogr.* **1952**, *5*, 356–361.

[24] A. Sumiyoshi, H. Hyodo, K. Kimura, *J. Phys. Chem. Solids* **2010**, *71*, 569–571.

[25] A. S. Golub, Y. V. Zubavichus, Y. L. Slovokhotov, Y. N. Novikov, *Russ. Chem. Rev.* **2003**, *72*, 123–141.

[26] D. Schild, S. Ulrich, J. A. Ye, M. Stuber, *Solid State Sci.* **2010**, *12*, 1903–1906.

[27] Y. Wang, Z. X. Shi, J. Yin, *J. Mater. Chem.* **2011**, *21*, 11371–11377.

[28] G. L. Frey, K. J. Reynolds, R. H. Friend, H. Cohen, Y. Feldman, *J. Am. Chem. Soc.* **2003**, *125*, 5998–6007.

[29] G. K. Wertheim, F. J. DiSalvo, D. N. E. Buchanan, *Phys. Rev. B* **1983**, *28*, 3335–3338.

[30] J. Y. Kim, S. M. Choi, W. S. Seo, W. S. Cho, *Bull. Korean Chem. Soc.* **2010**, *31*, 3225–3227.

[31] J. V. Acrivos, W. Y. Liang, J. A. Wilson, A. D. Yoffe, *J. Phys. C* **1971**, *4*, L18–L20.

